Possible Kondo Physics near a Metal-Insulator Crossover in the *A*-Site Ordered Perovskite $CaCu_3Ir_4O_{12}$

J.-G. Cheng,[1,2,3,*] J.-S. Zhou,[1] Y.-F Yang,[3] H. D. Zhou,[4] K. Matsubayashi,[2] Y. Uwatoko,[2] A. MacDonald,[5] and J. B. Goodenough[1]

[1]*Materials Science and Engineering Program and Texas Materials Institute, University of Texas at Austin, Austin, Texas 78712, USA*
[2]*Institute for Solid State Physics, University of Tokyo, Kashiwa 277-8581, Japan*
[3]*Beijing National Laboratory for Condensed Matter Physics, and Institute of Physics, Chinese Academy of Sciences, Beijing 100190, China*
[4]*Department of Physics and Astronomy, University of Tennessee, Knoxville, Tennessee 37996, USA*
[5]*Department of Physics and Texas Materials Institute, University of Texas at Austin, Austin, Texas 78712, USA*

(Received 3 June 2013; revised manuscript received 5 September 2013; published 23 October 2013)

The *A*-site ordered perovskite $(AA'_3)B_4O_{12}$ can accommodate transition metals on both A' and B sites in the crystal structure. Because of this structural feature, it is possible to have narrow-band electrons interacting with broadband electrons from different sublattices. Here we report a new *A*-site ordered perovskite $(CaCu_3)Ir_4O_{12}$ synthesized under high pressure. The coupling between localized spins on Cu^{2+} and itinerant electrons from the Ir-O sublattice makes Kondo-like physics take place at a temperature as high as 80 K. Results from the local density approximation calculation have confirmed the relevant band structure. The magnetization anomaly found at 80 K can be well rationalized by the two-fluid model.

DOI: 10.1103/PhysRevLett.111.176403 PACS numbers: 71.27.+a, 71.38.Cn, 75.20.Hr

Physical properties at the crossover from localized to itinerant electronic behavior remain poorly understood [1]. In simple ABO_3 perovskite oxides, for example, the electronic bandwidth is determined by *B*-O bond lengths and by *B*-O-*B* bond angles between distorted BO_6 octahedra. The localized-to-itinerant crossover can then be approached either by chemical substitution on the *A* site [2,3] or by applying high pressure [4,5]. The *A*-site ordered perovskite system $CaCu_3B_4O_{12}$ (B = transition metal) provides a richer example of this crossover because of the $3d$ electrons present on the A'-site Cu ions [6–17]. A'-and *B*-site transition metal orbitals in these systems can be coupled by strong covalent mixing with shared O^{2-} ions. We show in this paper that this coupling leads to peculiar properties suggestive of Kondo physics close to a metal-insulator transition.

In *A*-site-ordered perovskites containing Cu^{2+} ions, the *B*-O-*B* bond angle is much smaller than in typical ABO_3 perovskites as a result of the square-planar CuO_4 coordination preferred by the A'-site cations, which is illustrated in the inset of Fig. 1(b). The square-planar coordination stabilizes $3z^2$-r^2 and x^2-y^2 orbitals and leaves the xy orbital half-filled in the Cu:$3d^9$ configuration [18]. The behavior of the Cu^{2+} $3d$ holes can be tuned to be either localized or itinerant, depending on the B^{4+} transition-metal ion placed on the *B* site. The similarity of the local crystal environment as the high-T_c cuprates and the tunability of the Cu^{2+} electronic states makes them a clean system to gain insights into the cuprate electronic states [19]. However, the Cu electronic states at the localized-to-itinerant crossover, where the unconventional superconductivity emerges, remain unknown in the existing members of $CaCu_3B_4O_{12}$. Electronic structure variations with B^{4+}

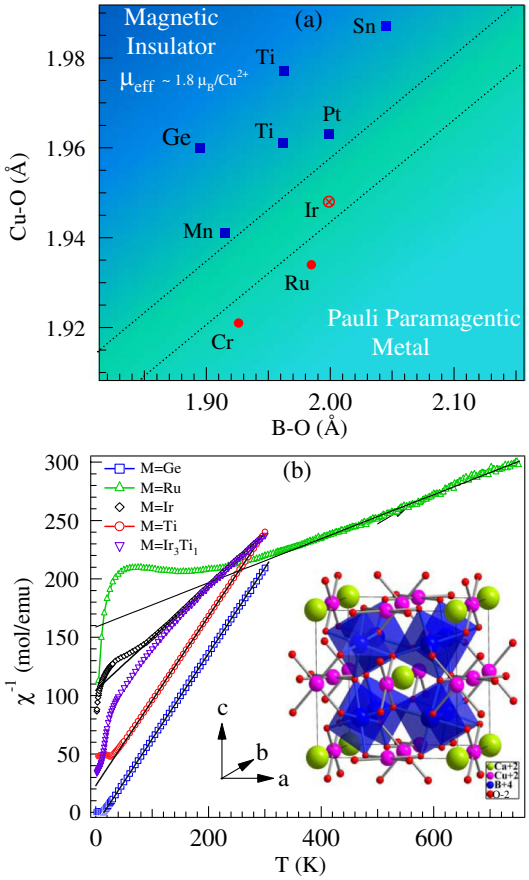

FIG. 1 (color online). (a) The Cu-O bond length in the coplanar CuO_4 versus *B*-O bond length in the octahedral BO_6 for *A*-site ordered perovskites $CaCu_3B_4O_{12}$. (b) The inverse magnetic susceptibility of several $CaCu_3B_4O_{12}$ perovskites. Inset: schematic crystal structure of the *A*-site ordered perovskite.

transition-metal ions are accompanied by corresponding crystal structure changes. In order to illustrate the correlation between bond lengths and electronic states, we have constructed a phase diagram in Fig. 1(a) in which the magnetic properties of a series of $CaCu_3B_4O_{12}$ compounds are correlated with Cu-O and B-O bond lengths. Here we see that the B^{4+} ions with an empty or full π-bonding d shell, such as Ti^{4+} $(3d^0)$[7,17], Pt^{4+} $(5t^6e^0)^8$, Ge^{4+} $(3d^{10})$[9,17], and Sn^{4+} $(4d^{10})$[9,17] have long Cu-O bonds and short B-O bonds and are insulating with a paramagnetic susceptibility $\mu_{\rm eff}$ close to the spin-only value of Cu^{2+} ($S = 1/2$). The only low-energy degrees of freedom in these materials reside on the Cu sites. On the other hand, d electrons on both Cu and the B ions become delocalized when the B-cation π-bonding d shell is partially filled as in V^{4+} $(3d^1)$[11], Cr^{4+} $(3d^2)$[12], and $Ru^{4+}(4t^4e^0)$[13–16]. $CaCu_3Ir_4O_{12}$, the subject of this work, is at the boundary separating these two areas in the structure phase diagram. Because of its strong spin-orbit coupling [20] Ir^{4+} $(5t^5e^0)$ can form a Mott insulator state in spite of its otherwise broad $5d$ bands. The results reported in this letter confirm that in $CaCu_3Ir_4O_{12}$, Cu exhibits neither simple itinerant-electron nor simple localized-electron behavior. The anomalous physical properties we report suggest Kondo behavior of Cu^{2+} moments coupled to Ir d orbitals that are close to a metal-insulator transition. The presence of many Ir bands at the Fermi energy in the local density approximation (LDA) calculations suggests strong-correlation behavior in which the Ir-ion degrees of freedom makes Hund's couplings [21] relevant. Moreover, since the Cu-O sublattice appears to be on the verge of the magnetic order that is expected to emerge when the Ir orbitals localize, the physical properties of $CaCu_3Ir_4O_{12}$ at low temperatures could be influenced by quantum critical fluctuations.

As summarized in Table S1 of the Supplemental Material [22], $CaCu_3Ir_4O_{12}$ requires high-pressure synthesis like most A-site ordered $CaCu_3B_4O_{12}$ perovskites. Details about the sample synthesis and characterizations can be found in the Supplemental Material [22].

If the electrons on the B-O sublattice are itinerant, as in $CaCu_3Ru_4O_{12}$, the character of the electronic states on the Cu sites is more successfully revealed by magnetic susceptibility fits than by transport measurements. Fig. 1(b) gives an overview of $\chi^{-1}(T)$ for known $CaCu_3B_4O_{12}$ compounds. Although $\chi^{-1}(T)$ is linear at $T > 330$ K in $CaCu_3Ru_4O_{12}$, the unphysically large Weiss constant indicates that the localized-electron Curie-Weiss (CW) law does not apply. We can therefore conclude that the electrons on both Cu^{2+} and Ru^{4+} sites are itinerant in this material. In contrast, for both $B =$ Ti and $B =$ Ge, fitting to a CW law gives not only a $\mu_{\rm eff}$ close to the spin-only value of a Cu^{2+} ion, but also a Weiss constant $|\theta_{\rm CW}| \sim T_N(T_c)$. Consistent with the structure-electronic-property correlations summarized in Fig. 1(a), the $\chi^{-1}(T)$ of $CaCu_3Ir_4O_{12}$ is located between the two extreme regimes; the Cu electrons behave like local moments at higher temperatures, before appearing to exhibit bandlike behavior at intermediate temperatures and enhanced magnetism to which we return below at the lowest temperatures. Since the contribution to $\chi(T)$ from the Ir^{4+} sublattice is relatively small in $SrIrO_3$ [23], we attribute the enhanced $\chi(T)$ at low temperature in Fig. 1(b) to a Cu^{2+} sublattice that is close to spin ordering. The $\chi(T)$ data also show that partial substitution of Ti^{4+} for Ir^{4+} tends to localize the Cu^{2+} electrons.

Figure 2 summarizes the physical properties measured on a $CaCu_3Ir_4O_{12}$ sample. The $\chi(T)$ measured at $H = 1$ T shows no signature of a magnetic ordering transition down to 1.8 K, but a clear deviation from the CW law below $T^* \approx 80$ K. A CW fit to $\chi^{-1}(T)$ between 100 and 300 K yields $\mu_{\rm eff} = 4.22\ \mu_B$/f.u. for the effective moment and $\theta_{\rm CW} = -232.5(7)$ K for the interaction parameter. This $\mu_{\rm eff}$ value is significantly larger than the spin-only value for Cu^{2+} since the contribution from the Ir-O sublattice should be negligible [24,25]. $CaCu_3Ir_4O_{12}$ is metallic down to 0.5 K. The susceptibility anomaly below T^* is echoed in $\rho(T)$, and also in the thermoelectric power $S(T)$. Above T^*, $\rho(T)$ follows a perfect linear T dependence; the data between 88 and 300 K can be fit well by $\rho = \rho_0 + A \times T$ with $\rho_0 = 2.729(1)$ mΩ cm and $A = 6.457(5)$ $\mu\Omega$ cm/K. Below T^*, $\rho(T)$ exhibits a strong downward trend with no sign of a curvature change down to 0.5 K, strongly suggestive of non-Fermi-liquid behavior. Although the resistivity anomaly develops at the same temperature as the magnetic susceptibility anomaly, we find that $\rho(T)$ is field independent up to $H = 5$ T (see Fig. S3 in the Supplemental Material [22]). The unusual temperature dependence of $\rho(T)$ below T^* cannot be explained in terms of the weak electron-electron and electron-phonon interactions of conventional metals. Significantly, $S(T)$ also behaves anomalously, changing sign at T^* and remaining large (-10 μV/K at around 5 K) as T approaches zero. The large thermoelectric power at low temperatures signals strongly energy-dependent quasiparticle properties. The absence of a corresponding anomaly in the specific heat $C(T)$, displayed in the form of C/T versus T in Fig. 2(d), rules out the possibility of a second-order phase transition at T^*. Interestingly, C/T of $CaCu_3Ir_4O_{12}$ exhibits a remarkable enhancement below $\sim$20 K. The absence of a corresponding enhancement in the closely related $SrIrO_3$ perovskite, which is a Pauli paramagnetic metal, indicates that this low-temperature anomaly must be associated with the Cu^{2+} $3d$ electrons or with interactions between Cu:$3d$ and Ir:$5d$.

The drop in $\rho(T)$ below $T^* = 80$ K is reminiscent of the low-temperature behavior in heavy-Fermion (HF) materials [26], and could suggest that the Cu^{2+} moments begin to be incorporated into the bands below this temperature. The presence of both Cu^{2+} $3d$ electrons and itinerant Ir^{4+} $5d$ electrons, which are likely to dominate transport in

$CaCu_3Ir_4O_{12}$, makes this analogy suggestive. In this picture, electrons on the two sublattices are weakly coupled above T^*. The initial reduction in $\chi(T)$ relative to the extrapolated CW fit at $T > T^*$ may signal the onset of hybridization of Cu electrons with the itinerant Ir^{4+} $5d$ electrons. The quick drop of $\rho(T)$ and the sign crossover of $S(T)$ at T^* appears to confirm the emergence of a hybridization between more localized electrons on Cu and more itinerant electrons on Ir. The incorporation of the Cu^{2+} $3d$ electrons into the itinerant bands would not only enhance the density of states, but also reduce the scattering from local magnetic moments. A field-independent $\rho(T)$ is consistent with the scenario of screened spins on the Cu sites. Indeed, $\chi(T)$ can be fit reasonably well over the entire temperature range by a *two-fluid* model [27]; see Fig. S4 in the Supplemental Material [22] for the details. In contrast to regular HF materials in which f electrons and d electrons are on the same atom, the hybridization between $3d$ electrons on Cu and $5d$ electrons on Ir of $CaCu_3Ir_4O_{12}$ must be mediated by shared O:$2p$ orbitals. Electronic hybridization should shorten Cu-O-Ir bond lengths and influence lattice dynamics. Strong bond-length fluctuations of this type below T^*, therefore, provide a natural explanation of the glassy (short phonon mean free path) thermal conductivity seen in $CaCu_3Ir_4O_{12}$, which is unique in the entire family of A-site ordered $CaCu_3B_4O_{12}$ perovskites. (See Fig. 2(e) and Fig. S5 of the Supplemental Material [22].)

Further evidence for the coherent incorporation of Cu local moments in the Ir bands can be found in the specific-heat measurement. In Fig. 3(a), $C(T)$ of $CaCu_3Ir_4O_{12}$ measured at $H = 0$ and at $H = 9$ T in the temperature interval 0.35–30 K is plotted in the form of C/T vs T^2. Figure 3(a) also displays the specific heat of several isostructural $CaCu_3B_4O_{12}$ (B = Ti, Mn, Ru, and V) compounds and the $SrIrO_3$ perovskite for comparison. The T-linear electronic specific-heat coefficient γ is negligible, as expected for insulating $CaCu_3B_4O_{12}$ compounds, with

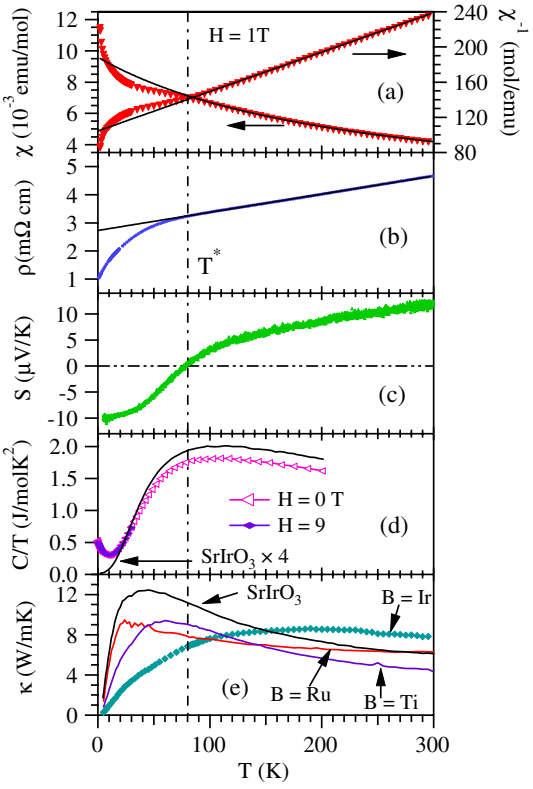

FIG. 2 (color online). Temperature dependence of (a) magnetic susceptibility $\chi(T)$ and its inverse $\chi^{-1}(T)$ measured under $H = 1$ T after zero-field cooling, (b) resistivity $\rho(T)$ under $H = 0$ T, (c) thermopower $S(T)$, (d) specific heat $C(T)$ under $H = 0$ and 9 T, and (e) thermal conductivity $\kappa(T)$ for $CaCu_3Ir_4O_{12}$. The solid line in (a) is a Curie-Weiss fitting curve to $\chi(T)$ between 100 and 300 K. The solid line in (b) is a linear fitting to $\rho(T)$ between 88 and 300 K. For comparison, $C(T)$ of the perovskite $SrIrO_3$ and $\kappa(T)$ of $CaCu_3B_4O_{12}$ (B = Ti, Ru) and $SrIrO_3$ were included in (d) and (e), respectively. $C(T)$ of $SrIrO_3$ was scaled by a factor of 4 in order to account for the difference of chemical formula. The vertical dotted line marks a characteristic temperature $T^* = 80$ K where the physical properties exhibit anomalies.

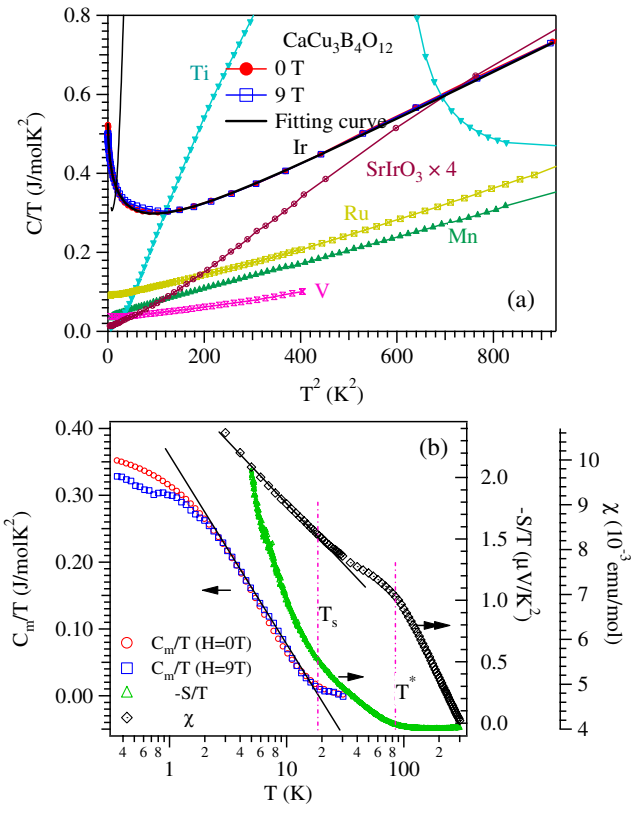

FIG. 3 (color online). (a) C/T versus T^2 of $CaCu_3Ir_4O_{12}$and isostructural $CaCu_3B_4O_{12}$ (B = Ti, Mn, V[11], Ru) as well as $SrIrO_3$ perovskite. (b) Logarithmic temperature dependences of C_m/T, $-S/T$, and $\chi(T)$ for $CaCu_3Ir_4O_{12}$. The solid line in (a) represents a fitting curve; see Supplemental Material [22] for details. Two characteristic temperatures $T^* = 80$ K and $T_s \approx 20$ K are marked by the dotted lines in (b).

B = Ti and Ge; γ increases significantly for the metallic perovskites with $B = V$ and Ru. A $\gamma = 173$ mJ/mol K^2, for $CaCu_3Ir_4O_{12}$ is much larger than that in $SrIrO_3$ and $CaCu_3Ru_4O_{12}$; see the Supplemental Material [22] for the detailed analysis of $C(T)$. Additionally, the dimensionless ratio that combines specific heat and thermoelectric power, $q = N_{Av}eS/\gamma T$ (N_{Av} is the Avogadro number and e the electron charge) has a value (-0.66) similar to that of Yb-based HF materials [28], which suggests transport and specific heat arise from the same degrees of freedom.

We note that there is a low-temperature rise in C_m/T; it is examined more closely in Fig. 3(b) and compared with similar increases in $\chi(T)$ and -S/T below 20 K. These observations could suggest that $CaCu_3Ir_4O_{12}$ is close to a magnetic quantum critical point since ordered Cu local moments are expected to emerge when the Ir d orbitals localize. In order to verify that $CaCu_3Ir_4O_{12}$ is close to a magnetically ordered phase, we have made partial substitutions of Ti^{4+} for Ir^{4+} in $CaCu_3(Ir_{1-x}Ti_x)_4O_{12}$. The magnetization M($T$) for $x = 0.25$ of Fig. S7 in the Supplemental Material [22] indeed reveals a broad transition to a spin ordered phase below 40 K. The γ from the paramagnetic phase for the $x = 0.25$ sample is close to that of the $x = 0$ sample. Instead of a typical λ peak, $C(T)$ is enhanced on top of a broad base. However, the low-temperature upturn is clearly absent. As for the $x = 0.375$ sample, the magnetic transition looks like that of a filamentary phase of the $x = 1$ sample, and no enhancement of $C(T)$ can be observed.

This picture is partially supported by LDA calculations based on the full-potential linearized augmented plane-wave method as implemented in the WIEN2K code [29]. In Fig. 4(a), our LDA results for the partial density of states show that four of the five Cu 3d orbitals are fully occupied and clustered around 2 eV below the Fermi energy. Only the d_{xy} orbital is partially occupied. The Ir 5d orbitals, all of which cross the Fermi energy in our calculations, and the Cu d_{xy} orbital are responsible for all the observed electronic properties. The Cu d_{xy} orbital and Ir 5d orbitals are strongly hybridized via O-p orbitals. The band structures shown in Fig. 4(b) reveal a complicated hybridization pattern: effectively, only two of the three Cu d_{xy} orbitals in the unit cell form covalent bonding states with the Ir and O orbitals; the third flat Cu d_{xy} band at around 0.2 eV above the Fermi energy crosses and hybridizes with a very dispersive Ir hole band. This feature of the band structure may be responsible for the unusual temperature dependence of the resistivity above T^*. Our LDA calculations give $\gamma = 17$ mJ/mol K^2 much smaller than $\gamma = 173$ mJ/mol K^2 from experiment, demonstrating that the electronic specific heat is strongly enhanced by electronic correlations.

Another important finding from the LDA calculations is that both σ and π bonds at Ir sites contribute to the density of states at E_F. This feature suggests that intra-atomic interactions, including Hund's exchange, may play a role in the strong Ir correlations, in addition to the Coulomb energy U, just as multiple band crossings at E_F are thought to complicate the correlation physics of iron-based pnictide superconductors. Haule and Kotliar [30] have shown, for example, that Hund's coupling in a metal can on its own cause a coherent to incoherent crossover which leads to anomalies in both resistivity $\rho(T)$ and susceptibility $\chi(T)$.

In conclusion, the peculiar crystal structure of A-site-ordered perovskite $CaCu_3Ir_4O_{12}$ leads to coupling between the Cu local moment system and the Ir-O system that is

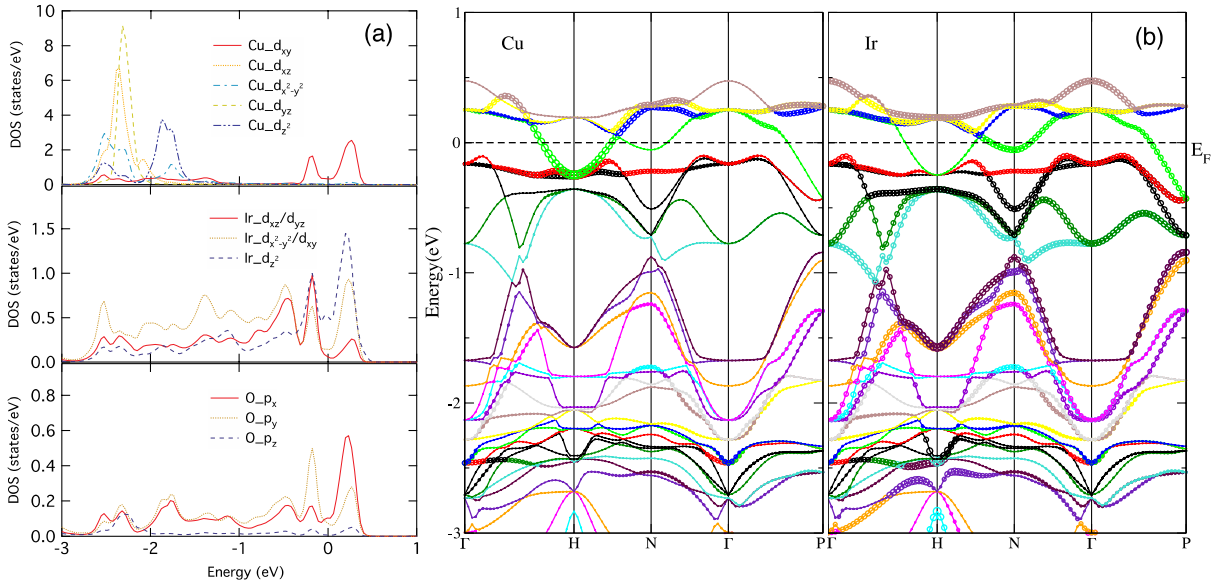

FIG. 4 (color online). LDA calculations for (a) the partial density of states and (b) the band structures for the Cu d_{xy} bands and all Ir d bands.

close to a metal-insulator transition and to a peculiar set of electronic properties. The coupling destroys magnetic order of the Cu local moments that appear to be incorporated in the Ir-O bands, leading a strongly enhanced electronic specific heat as in a heavy-Fermion compound. Measurements of specific heat, magnetic susceptibility, and thermoelectric power at low temperatures show non-Fermi-liquid behavior suggestive of nearby quantum critical behavior. Above a crossover temperature $T^* = 80$ K, the more extended $5d$ electrons on Ir and more narrow-band $3d$ electrons on Cu appear to decouple. The magnetization anomaly at 80 K can be well rationalized by the two-fluid model. As in iron-based pnictide superconductors, multiple bands cross the E_F in LDA calculations, suggesting that interactions between different atomic configurations play a role in Ir correlations.

Work at UTA was supported by NSF (DMR 1122603) and by the Robert A. Welch Foundation (Grant No. F-1066). Work at ISSP, University of Tokyo was partially supported by Grant-in-Aid for Scientific Research, KAKENHI (Grants No. 23340101 and No. 252460135). J. G. C. greatly acknowledges the financial support of the JSPS fellowship for foreign researchers (Grant No. 12F02023), the National Basic Research Program of China (973 program, Grant No. 2014CB921500), and the Chinese Academy of Sciences (Grant No. Y2K5016X51). Y. F. Y. is supported by NSF-China (Grant No. 11174339) and by the Chinese Academy of Sciences. K. M. is supported by Grant-in-Aid for Young Scientist B (No. 24740220) from the Ministry of Education, Culture, Sports, Science and Technology, Japan. J. G. C. is grateful to J. Q. Yan for enlightening discussions.

*jgcheng@iphy.ac.cn

[1] J. B. Goodenough, *Localized to Itinerant Electronic Transition in Perovskite Oxides*, Structure and Bonding, Vol. 98 edited by J. B. Goodenough (Springer, Berlin, Germany, 2001).
[2] J. S. Zhou, W. Archibald, and J. B. Goodenough, Phys. Rev. B **61**, 3196 (2000).
[3] J.-S. Zhou, C.-Q. Jin, Y.-W. Long, L.-X. Yang, and J. B. Goodenough, Phys. Rev. Lett. **96**, 046408 (2006).
[4] J.-S. Zhou, J. B. Goodenough, and B. Dabrowski, Phys. Rev. Lett. **94**, 226602 (2005).
[5] J.-S. Zhou and J. B. Goodenough, Phys. Rev. Lett. **89**, 087201 (2002).
[6] Y. Shimakawa, Inorg. Chem. **47**, 8562 (2008).
[7] Y. Shimakawa, H. Shiraki, and T. Saito, J. Phys. Soc. Jpn. **77**, 113702 (2008).
[8] I. Yamada, Y. Takahashi, K. Ohgushi, N. Nishiyama, R. Takahashi, K. Wada, T. Kunimoto, H. Ohfuji, Y. Kojima, T. Inoue, and T. Irifune, Inorg. Chem. **49**, 6778 (2010).
[9] H. Shiraki, T. Saito, T. Yamada, M. Tsujimoto, M. Azuma, H. Kurata, S. Isoda, M. Takano, and Y. Shimakawa, Phys. Rev. B **76**, 140403(R) (2007).
[10] Z. Zeng, M. Greenblatt, M. A. Subramanian, and M. Croft, Phys. Rev. Lett. **82**, 3164 (1999).
[11] H. Shiraki, T. Saito, M. Azuma, and Y. Shimakawa, J. Phys. Soc. Jpn. **77**, 064705 (2008).
[12] M. A. Subramanian, W. J. Marshall, T. G. Calvarese, and A. W. Sleight, J. Phys. Chem. Solids **64**, 1569 (2003).
[13] W. Kobayashi, I. Terasaki, J. Takeya, I. Tsukada, and Y. Ando, J. Phys. Soc. Jpn. **73**, 2373 (2004).
[14] A. Krimmel, A. Gunther, W. Kraetschmer, H. Dekinger, N. Buttgen, V. Eyert, A. Loidl, D. V. Sheptyakov, E.-W. Scheidt, and W. Scherer, Phys. Rev. B **80**, 121101 (R) (2009).
[15] T. T. Tran, K. Takubo, T. Mizokawa, W. Kobayashi, and I. Terasaki, Phys. Rev. B **73**, 193105 (2006).
[16] A. Krimmel, A. Gunther, W. Kraetschmer, H. Dekinger, N. Buttgen, A. Loidl, S. G. Ebbinghaus, E.-W. Scheidt, and W. Scherer, Phys. Rev. B **78**, 165126 (2008).
[17] Y. Shimakawa and T. Saito, Phys. Status Solidi B **249**, 423 (2012).
[18] H. Xiang, X. Liu, E. Zhao, J. Meng, and Z. Wu, Phys. Rev. B **76**, 155103 (2007).
[19] D. Meyers, S. Mukherjee, J.-G. Cheng, S. Middey, J.-S. Zhou, J. B. Goodenough, B. A. Gray, J. W. Freeland, T. Saha-Dasgupta, and J. chakhalian, Sci. Rep. **3**, 1834 (2013).
[20] B. J. Kim, H. Jin, S. J. Moon, J.-Y. Kim, B.-G. Park, C. S. Leem, J. Yu, T. W. Noh, C. Kim, S.-J. Oh, J.-H. Park, V. Durairaj, G. Cao, and E. Rotenberg, Phys. Rev. Lett. **101**, 076402 (2008).
[21] A. Georges, L. d. Medici, and J. Mravlje, Annu. Rev. Condens. Matter Phys. **4**, 137 (2013).
[22] See Supplemental Material at http://link.aps.org/supplemental/10.1103/PhysRevLett.111.176403 for sample synthesis, structural characterization, magnetoresistance, and fitting to the specific heat and magnetic susceptibility.
[23] J.-G. Cheng, J.-S. Zhou, J. B. Goodenough, Y. Sui, Y. Ren, and M. R. Suchomel, Phys. Rev. B **83**, 064401 (2011).
[24] G. Cao, J. Bolivar, S. McCall, J. E. Crow, and R. P. Guertin, Phys. Rev. B **57**, R11039 (1998).
[25] G. Cao, J. E. Crow, R. P. Guertin, P. F. Henning, C. C. Homes, M. Strongin, D. N. Basov, and E. Lochner, Solid State Commun. **113**, 657 (2000).
[26] Y.-F. Yang, Z. Fisk, H.-O. Lee, J. D. Thompson, and D. Pines, Nature (London) **454**, 611 (2008).
[27] Y.-F. Yang and D. Pines, Proc. Natl. Acad. Sci. U.S.A. **109**, E3060 (2012).
[28] K. Behnia, D. Jaccard, and J. Flouquet, J. Phys. Condens. Matter **16**, 5187 (2004).
[29] P. Blaha, K. Schwarz, G. K. H. Madsen, D. Kvasnicka, and J. Luitz, *WIEN2K, User's Guide* (Technische Universitat Wien, Austria, 2001), http://www.wien2k.at/reg_user/textbooks/usersguide.pdf.
[30] K. Haule and G. Kotliar, New J. Phys. **11**, 025021 (2009).